Modelling of Crack-Face Interference Free Biaxial Crack Propagation in Smooth Normalized SAE 1045 Steel Tubes

John J.F. Bonnen[1] **and Timothy H. Topper**[2]

[1]Research Staff, Ford Motor Co., MD3135 RIC, P.O.B. 2053, Dearborn, MI, 48121 USA
[2]Department of Civil Eng., University of Waterloo, Waterloo, Ontario, Canada, N2L 3G1

ABSTRACT. *A series of in-phase axial-torsional smooth tube fatigue experiments were performed using regular intermittent overloads in otherwise constant amplitude load histories to achieve crack-face interference-free (crack closure free) fatigue crack growth. Observations were made of not only the fatigue life but if and when the initial crack growth on a plane of maximum shear stress range changed to crack growth on a plane of maximum tensile stress range. Although there was a considerable scatter in the strain and length at which changes in crack growth mode occurred, the general trend in the data was that the crack length at which change occurred increased with increasing strain and strain ratio. Two separate criteria for crack growth mode change from shear plane to tensile plane crack growth were inserted into a strain based short crack fatigue crack growth model. When the crack length at the change in mode was predicted using the first criterion (based on choosing the plane that exhibited the maximum crack growth rate) the boundary, which is formed on a strain versus crack length plot, fell at lower strains than the data. Use of the other criterion (based on choosing the plane with the higher strain energy release rate) yielded a boundary that indicated shorter than observed crack lengths and an upper bound to the strain at which changes in mode were observed. Fatigue lives predicted using the two forms of the model fell very close to each other and to the experimental fatigue life data. The closeness in the life predictions produced by the two forms of the model and the scatter in observed strain and crack length at the point of mode change are assumed to be a consequence of nearly equal crack growth rates for tensile and shear mode crack growth.*

INTRODUCTION

In the early 1970's Elber [1, 2] demonstrated that crack closure substantially reduces the mode I crack driving force seen at the crack tip, and a similar concept, crack-face interference, has extended this idea to include modes II and III. In this paper we present cracking mode and fatigue life information for crack face interference free smooth tube fatigue life tests. Also changes in cracking mode and fatigue life are predicted using a short crack growth model and interference free mode I and II crack growth rate data.

Although eliminating crack-face interference is difficult to achieve, two techniques have been successfully used – the application of sufficiently large constant tensile stresses

normal to the crack face [3, 4, 5, 6] (under mode I loading this means very high mean stresses) and the periodic insertion into a constant amplitude stress history of very large overloads (on the order of the net section yield stress) either normal to [5, 7] or in the plane of the growing crack [5, 8, 9]. The first technique keeps the crack faces apart, and the second technique, depending on how it is employed, keeps the crack faces apart and/or crushes existing crack face asperities flat so that they no longer hinder crack growth. Once crack-face interference has been eliminated we obtain the most conservative possible fatigue curve for a given material.

These techniques were used by the present authors to develop a series of biaxial crack-face interference-free strain-life fatigue curves for normalized SAE 1045 steel for five different but constant biaxial strain ratios ($\lambda = \varepsilon_{xy}/\varepsilon_{xx} = 0$, 3/4, 3/2, 3 and ∞.) [8]. Observation of the paths that the growing (crack-face interference-free) fatigue cracks took in the tubes revealed consistent behavior. Cracks initiated on planes of maximum shear strain range, grew for a distance on these planes and then, in some cases, changed to growth on planes of maximum tensile strain range. The length of the shear crack at which the change from shear to tensile plane growth occurred depended on the small cycle strain amplitude and the biaxial strain ratio: increasing either the amplitude or the ratio led to increasing shear crack lengths, and often led to a shear crack which spanned the specimen gage length. Even so, for given values of the strain amplitude and the biaxial strain ratio, the observed maximum shear crack lengths varied substantially.

MATERIAL, PROCEDURES, AND EXPERIMENTAL RESULTS

In this investigation a normalized SAE 1045 steel with a nominal hardness of 203 BHN, previously the focus of an SAE Fatigue Design and Evaluation Committee multiaxial fatigue study [10, 11], was used in both crack growth and fatigue life experiments. It has a ferritic-pearlitic microstructure which is moderately banded longitudinally resulting in ferrite-rich channels (in which fatigue cracks tended to grow) and pearlite rich channels. The grains are roughly equiaxed and average $25\mu m$ in diameter. Microstructure and mechanical properties are detailed in [12].

All specimens were machined such that the rolling direction was parallel to the long axis of the specimen. Details of specimen design, preparation and testing of the smooth unnotched axial dogbone and biaxial tubular specimens are given in references [8, 13].

Mode I crack-face interference-free crack growth testing was conducted on axial single edge notched specimens. Mode II crack-face interference-free crack growth testing was conducted on the biaxial tubular specimens used in the fatigue life experiments but with a 0.25mm diameter hole drilled through the 2.54mm tube wall acting as a central notch. All specimens were given a final longitudinal $5\mu m$ polish. All testing was conducted using computer control at frequencies ranging from 1-40Hz for biaxial specimens and 1-100Hz for axial specimens. Periodic overload histories, such as that found in the insets in Figure 1a and b, were used in both the fatigue life testing and in most of the crack growth testing. Further details of crack growth testing can be found in reference [12].

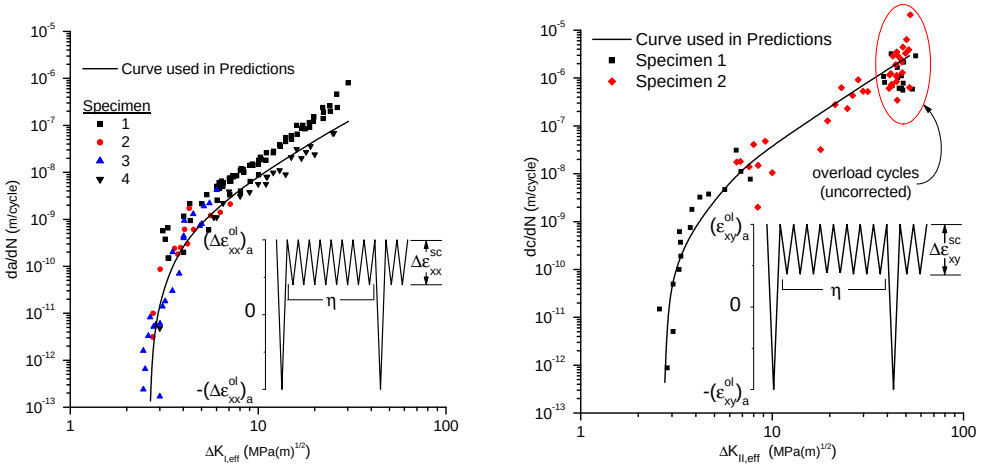

(a) Mode I fully effective long crack data (b) Mode II fully effective long crack data

Figure 1. Effective (Mode I crack closure free or Mode II crack-face interference-free) crack growth curves for normalized SAE 1045 steels.

Four SEN specimens were used to generate the crack closure-free long crack growth data plotted in Figure 1a. Two tubular crack growth specimens were used to produce the crack-face interference-free long crack growth curve in Figure 1b. Trend lines inscribed on the data are the piecewise linearized crack growth curves used in modelling.

CRACK GROWTH MODELS

Two versions of a single short crack growth model that used different algorithms to predict the shear crack length at which the crack growth mode changed from shear to tensile were used to predict the total fatigue lives and these transitions. These models were termed the "area" and "energy" models after the two crack path selector algorithms used to decide the change in crack growth plane. As well as these two different crack path selectors the model used a strain intensity based short crack growth equation, separate surface strain concentration factors for shear and tension modes, and different geometry factors for each of the three crack growth modes. For stress intensity calculations, a crack length projection technique was used to map the shear crack length into an equivalent tensile crack length at the point of changeover in growth mode and during evaluation of the crack path selector algorithm.

For all of the models cracks were assumed to begin as shallow surface cracks (or persistent slip bands – PSB's) of $3\mu m$ deep by $100\mu m$ long (a by $2c$), based on work in reference [9]. Observations of crack initiation in smooth tubes indicated that these cracks were oriented along the plane of maximum shear, except for those ratios ($\lambda = 3$ and 3/2) in which the shear cracks grew in the longitudinal ferrite channels. Further, cracks were observed to nucleate on the outer surface of the tube and grow inward. The model predicts that, as the crack grows, it shape changes from the initial very shallow, elliptical crack front toward a penny shape. Once the shear crack has grown through the first grain,

a depth of $25\mu m$, the model is allowed to decide whether to change to crack growth on to a plane of maximum tensile stress. When a tensile crack intersects the inner wall of the tube ($a = 2.54mm$), it is assumed to change immediately into a through crack in the tube with a surface crack length equal to the outer surface crack length. Failure is assumed to occur when the through crack reaches a length $2c_f = 30mm$ (the tube gage length). If the model predicted a growth mode change to growth on a tensile plane, it always occurred at a crack depth of less than $300\mu m$.

The same study [9] from which the initial crack size was drawn also found that shear cracks would predominantly grow in depth until about 80% of the total fatigue life was reached. At that juncture the cracks started to grow in length and rapidly linked up with adjacent shear cracks to form very long shear cracks. In the models a $300\mu m$ depth corresponded to roughly 80% of the fatigue life for strain amplitudes above the fatigue limit at all strain ratios. Thus in the model it is assumed that, at a crack length of $300\mu m$, a shear mode crack links up with other similar shear mode cracks to form a crack that spans the gage length. The shear crack then continues to grow until it penetrates the tube wall.

The experimental data from reference [12] was used to develop a ten piece linear approximation of the mode I crack growth data (Figure 1a) and an eleven piece linear approximation of the mode II crack growth data (as seen in Figure 1b) that were used in modelling. The latter curve was used for both modes II and III crack growth.

Crack Growth into the Tube Wall

In the first portion of the biaxial crack growth modelling, stress intensity equations suggested by Socie, et al. [14] were modified into a strain intensity form (first suggested by McEvily [15]):

$$\begin{aligned} \Delta K_I(\varepsilon) &= Q^t_\varepsilon \Delta e_{11} E F_I \sqrt{\pi c} \\ \Delta K_{II}(\varepsilon) &= Q^s_\varepsilon 2\Delta e_s G F_{II} \sqrt{\pi c} \\ \Delta K_{III}(\varepsilon) &= Q^s_\varepsilon 2\Delta e_s G F_{III} \sqrt{\pi c} \end{aligned}$$

where c is the surface half crack length, E (G) is the elastic (shear) modulus, and F is the crack geometry factor. In this formulation the tensorial shear strain on the shear crack growth plane ($\Delta e_s = \{\Delta e_{xy} \text{ or } \Delta e_{12}\}$) is half of the engineering strain ($e_s = \gamma_s/2$). The local strain at the surface (ε) is related to the bulk strain (e) by Q_ε, the surface strain concentration function proposed by Abdel-Raouf, et al. [16, 17]. This function captures the influence of the near surface stress state in which the crack initially grows, and is of the form $Q_\varepsilon = \frac{\Delta\varepsilon}{\Delta e} = 1 + q\exp(-a\alpha/D)$, where a is the crack depth, D the grain diameter, $\exp()$ is the natural exponent, and q and α are material constants. The expression for Q_ε is calibrated by adjusting α/D until the model correctly predicts the fatigue limit. The tensile concentration factor, Q^t_ε, was calibrated using a mode I crack growth model (a penny shaped crack in a rod under tension [18] with an aspect ratio (a/c) of 0.8 taken from fracture surface measurements and a failure crack length of $a_f = 5.08mm$), crack-face interference-free mode I crack growth data, and uniaxial fatigue life data. The value of α/D for tensile cracking was determined to be 105,000. The shear Q^s_εrequired a value of α/D of 45,000 to match the torsional fatigue limit ($\lambda = \infty$). In this latter calibration a

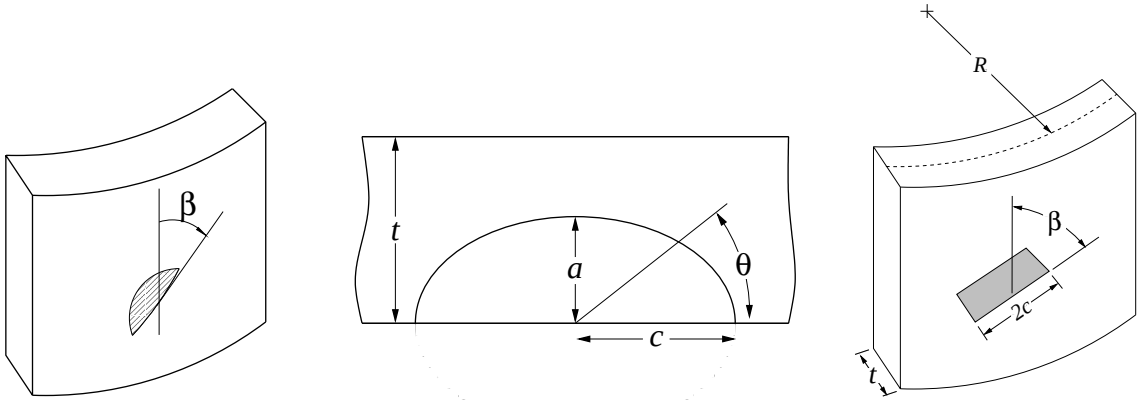

(a) Exterior elliptical surface crack. (b) Through-wall crack.

Figure 2. Definitions for a, c, β, θ, t, and R for a tube under axial-torsional loading.

form of the crack growth model was used that assumes continuous shear crack growth on planes of maximum shear strain and employs the mode II and mode III geometry factors.

Geometry Factors for an Elliptical Surface Crack

Geometry factors (F_I, F_{II}, and F_{III}) for an embedded elliptical crack of arbitrary shape subjected to a tensile stress normal to the crack plane and a shear stress applied along its major axis were used to model initial crack growth through the tube wall [19, 20, 21]. Versions of the mode I and mode II geometry factors, suitably modified for surface crack applications [14] by a $1.12\times$ multiplier, were used in the models. Curve fits made to the numerical solutions of the elliptical integrals (from *CRC Standard Mathematical Tables*) were used in the crack growth analyses. Figure 2a defines crack lengths a and c, the crack inclination angle (β), the parametric angle (θ) which defines the location along the crack front where the geometry factors are calculated, the tube wall thickness (t), and, R, the tube radius to mid-wall. The geometry factor causes the crack to evolve from the initial shallow elliptical shape ($a/c = 3/50 = 0.06$) toward a half-penny shaped crack ($a/c = 1$) (which is numerically stable once achieved). This behavior of the model is consistent with both the present fracture surface observations and measurements made by others [9].

A shear crack grows under mode II along the surface and mode III into the depth. The mixture of mode II and mode III at other points is a function of the the angle the crack front makes with the line of shear. Conversely, a crack growing on a plane of maximum tension is subject to only mode I loading. Thus, in the model cracks growing on planes of maximum shear use F_{II} and F_{III}, and cracks growing on planes of maximum tension use F_I.

A Through-Wall Tensile Crack Growing in a Tube

The transition from a surface crack to through crack is assumed to happen instantaneously once the deepest portion of the crack reaches the inner wall of the tube, and at that time it is assumed to become a through crack with the appearance shown in Figure 2b. This

λ	Crack Angle		
$\frac{\varepsilon_{xy}}{\varepsilon_{xx}}$	β	ϕ	β'
∞	0°	45°	45°
3	0°	52°	52°
3/2	0°	57°	57°
3/4	22.5°	45°	67.5°
0	45°	45°	90°

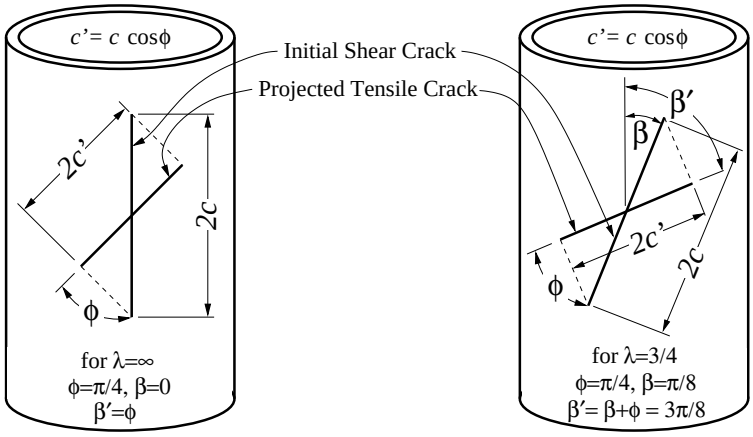

Figure 3. Crack length projection from shear plane onto tensile plane. ($\lambda = 0$ not modelled)

transition presumes that the remaining uncracked material is cracked in the last cycle to create a through crack of length $2c$. No backface correction factors were used.

The mode I stress intensity factor for an arbitrarily oriented through-crack were determined from the work of Lakshminarayana and Murthy [22]. Figure 2b shows the model geometry, and the general form of the strain intensity equation is

$$\Delta K_I(\varepsilon) = \Delta e_{xx} E \sqrt{\pi c}\left[\sin^2\beta + \frac{\pi\rho^2}{32}(3 - 2\cos 2\beta - \cos 4\beta)\right] + 2\Delta e_{xy} G \sqrt{\pi c}\left[\sin 2\beta + \frac{\pi\rho^2}{32}(9\sin 2\beta + 2\sin 4\beta)\right],$$

where $\rho^2 = \sqrt{12(1-\nu^2)}c^2/(8Rt)$ and ν is Poisson's ratio. The crack was grown to failure length using this model ($c = 15mm$).

Determining the Equivalent Tensile Crack Length

As mentioned before, the crack orientation algorithms determine whether the crack changes from growth on a plane of maximum shear to a plane of maximum tension. The crack length projection technique, illustrated in Figure 3 , was developed to convert the mode II surface crack length to an equivalent mode I surface crack length. The angle that the shear growth plane makes with the tube axis, β, is different from the angle that the plane of tension makes with the tube axis, β', by the angle ϕ. The length of the crack after conversion to the tensile plane, c', is related to the length of the shear crack, c, by the amount $c' = c\cos\phi$. This new surface crack length (c') is used for mode I strain intensity calculations for tensile growth. If a change is made, this new crack length is used for all future calculations. The material's preference for easy shear crack growth in the ferrite rich channels which run parallel to the longitudinal specimen axis [8] is reflected by the $\beta = 0°$ entries in the table in Figure 3 for strain ratios of $\lambda = 3$ and 3/2.

Crack Path Algorithms

After one grain diameter ($25\mu m$) of crack growth on planes of maximum shear strain amplitude and every subsequent crack growth increment, the model determines whether or not to change to growth on a plane of maximum tensile strain amplitude. This determination is made via a ratio given by the algorithms described below. The algorithms below are derived for an elliptical crack case.

Energy Criterion

The strain energy release rate criterion, developed by Palaniswamy and then Nuismer [23, 24], and based on fracture work by Griffith [25], posits that a crack will propagate in the direction in which the strain energy release rate is the greatest. In general terms, it may be expressed as $G_c = K^2/E = (F\Delta\sigma)^2\pi a/E = (FE\Delta\varepsilon)^2\pi a/E$, or, in terms of the incremental energy released by a given crack increment δa, it is $\delta G_c = (F\Delta\varepsilon)^2 E\pi\delta a$. Integration of $\delta G_{c,II}$ and $\delta G_{c,III}$ over θ leads to the total energy released per cycle under shear crack growth,

$$\delta G_c^s = 2G(Q_\varepsilon^s \Delta e_s)^2\pi\left((F_{III})^2\delta a_s + \frac{(F_{II})^2}{1+\nu}k\delta c_s\right),$$

where the sub/superscripts s and t indicate shear and tensile growth, respectively and Δe_s is the shear strain range on the active shear crack growth plane (as per Figure 3) and takes the value Δe_{xy} for $\lambda \geq 3/2$ and Δe_{12} otherwise. Similarly, for a growing tensile crack the incremental mode I energy released is $\delta G_c^t = E(Q_\varepsilon^t \Delta e_{11})^2\pi\left((F_I^a)^2\delta a_t + (F_I^c)^2 k\delta c_t\right)$, where F_I^a and F_I^c are the instantaneous mode I geometry factors in the a and c directions, respectively. Thus in the model, the ratio of the energies is defined as $\chi = \delta G_c^t/\delta G_c^s$.

Area Criterion

The area model was an extension of an observation by Hourlier and Pineau [26] that cracks grow in the mode in which the growth rates are highest. For the purpose of this work the criterion was restated as; a crack will grow in the direction in which the crack surface area increment is greatest. Thus, given different increments in the a and c directions in an elliptical crack, the area increment in crack growth is $\Delta A = \frac{\pi}{2}(c\Delta a + a\Delta c)$. The ratio for the area criterion is thus $\xi = \frac{\Delta A_t}{\Delta A_s} = \frac{c_t\Delta a_t + a\Delta c_t}{c_s\Delta a_s + a\Delta c_s}$.

CRACK GROWTH TRANSITION PREDICTIONS

Estimates of the maximum shear crack length before changing over to crack growth on tensile planes provided by the area and energy models are plotted in Figure 4 together with experimental observations . In the experiments a large number of tests did not exhibit a change from shear crack growth over to tensile crack growth. Conversely, another significant number of tests had no post mortem observable initiating shear crack. There were several cases where the initial shear crack changed over to crack growth on a tensile

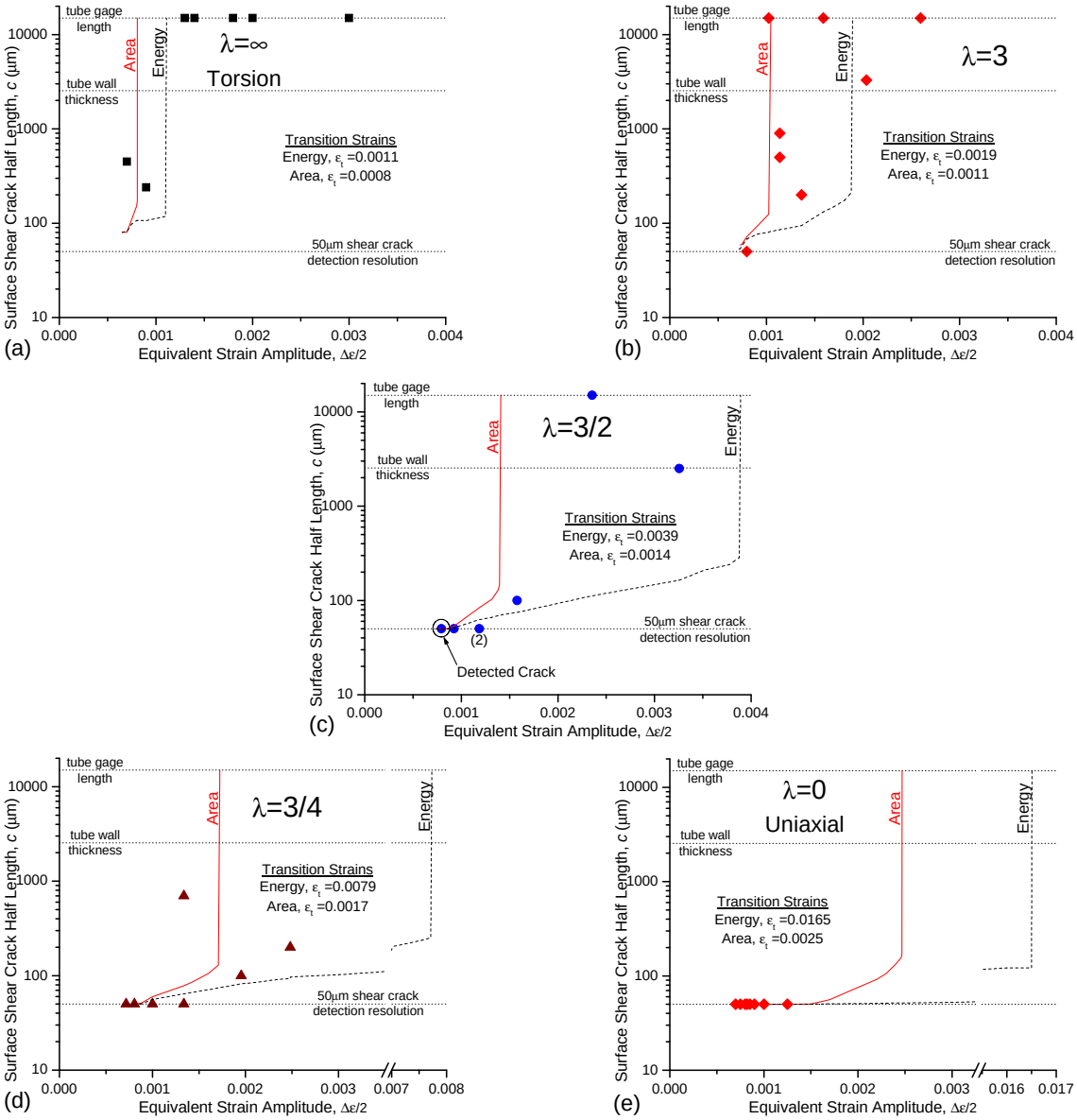

Figure 4. Experimental observations and predictions of maximum shear crack lengths (before crack growth changes to maximum tensile planes). For strains which exceed the transition strain (ε_t), models predict a shear crack that grows until it spans the gage length ($2c = 30mm$).

plane and then back again to growth on a shear plane – in these cases it is the initial shear crack half-length at the change in cracking mode that is plotted. With the exception of a single test ($\lambda = 3/2,\ \Delta\bar{\varepsilon}_{\text{eff}}/2 = 0.0008$) all of the tests plotted at the $50\mu m$ detection limit had initial shear cracks that were not detected. While the experimental data in the figure has a significant amount of scatter, it does show that the material exhibits increasingly longer shear cracks as shear the strain amplitude and the biaxial strain ratio increase.

Each of the two crack growth mode transition models predicts that above a certain

effective strain amplitude, labelled in Figure 4 as the transition strain amplitude, there will be no transition to crack growth on a tensile plane and cracks will grow to in shear. Below the transition strain both models predict a decrease in the crack length at the transition as the strain amplitude decreases until the assumed initial crack length of $50\mu m$ is reached. The boundaries given by the energy model fall at shorter crack lengths and higher strain amplitudes than those given by the area model. The measured crack growth mode transitions show a considerable amount of scatter but follow the trends predicted by the models – the maximum shear crack length increases as the strain amplitude and the strain ratio increase. Most of the data show a change from shear to tensile mode crack growth at strain amplitudes and lengths greater than the boundary predicted by the area model. The energy model on the other hand predicts a boundary that, in crack length, falls below almost all the data and in transition strain falls beyond the data.

FATIGUE LIFE PREDICTIONS

Fatigue life predictions are plotted together with experimental strain-life fatigue data in Figure 5 . Curves are shown for the “tensile,” “shear,” area, and energy fatigue life predictions. The "tensile" and "shear" predictions were made with the same basic models as the area and energy models were but had the crack growth mode confined to tensile plane growth in the first case, and to shear plane growth in the second. The “shear” model has an α/D value calibrated to predict the torsional fatigue limit (the same value is used by the area/energy models – see the “shear/calibration” curve, $\lambda = \infty$). The curves for the area and energy models almost coincide with the “shear” curve for $\lambda = \infty$ presumably because, as was shown in Figure 4a, they predict mainly shear growth.

At the other extreme of the strain ratios examined was uniaxial straining, and for this strain ratio the experimental fatigue data was produced with solid cylindrical specimens rather than with tubular specimens. The “tensile” model employed an α/D value calibrated to the uniaxial fatigue limit with a mode I penny crack ($a/c = 0.8$) in a solid cylinder (“tensile calibration” curve, Figure 5e). The “tensile” model and the area and energy models yield good, almost identical, predictions of the uniaxial fatigue life data. As shown in Figure 4e, the area and energy models predominately predict the same tensile mode growth used as a basis for the “tensile” model.

For the stress ratios between the torsion and the uniaxial extremes (Figures 5b-d), the “shear” model predictions improve as the strain ratio increases and, simultaneously, the “tensile” model predictions change from conservative to unconservative. The area and energy models predict curves that fall very close to each other for all strain ratios and yield consistently conservative, but good, fatigue life estimates.

DISCUSSION

The large differences in the predicted maximum shear crack length between the area and energy models appear to arise from small differences between mode I and II crack growth

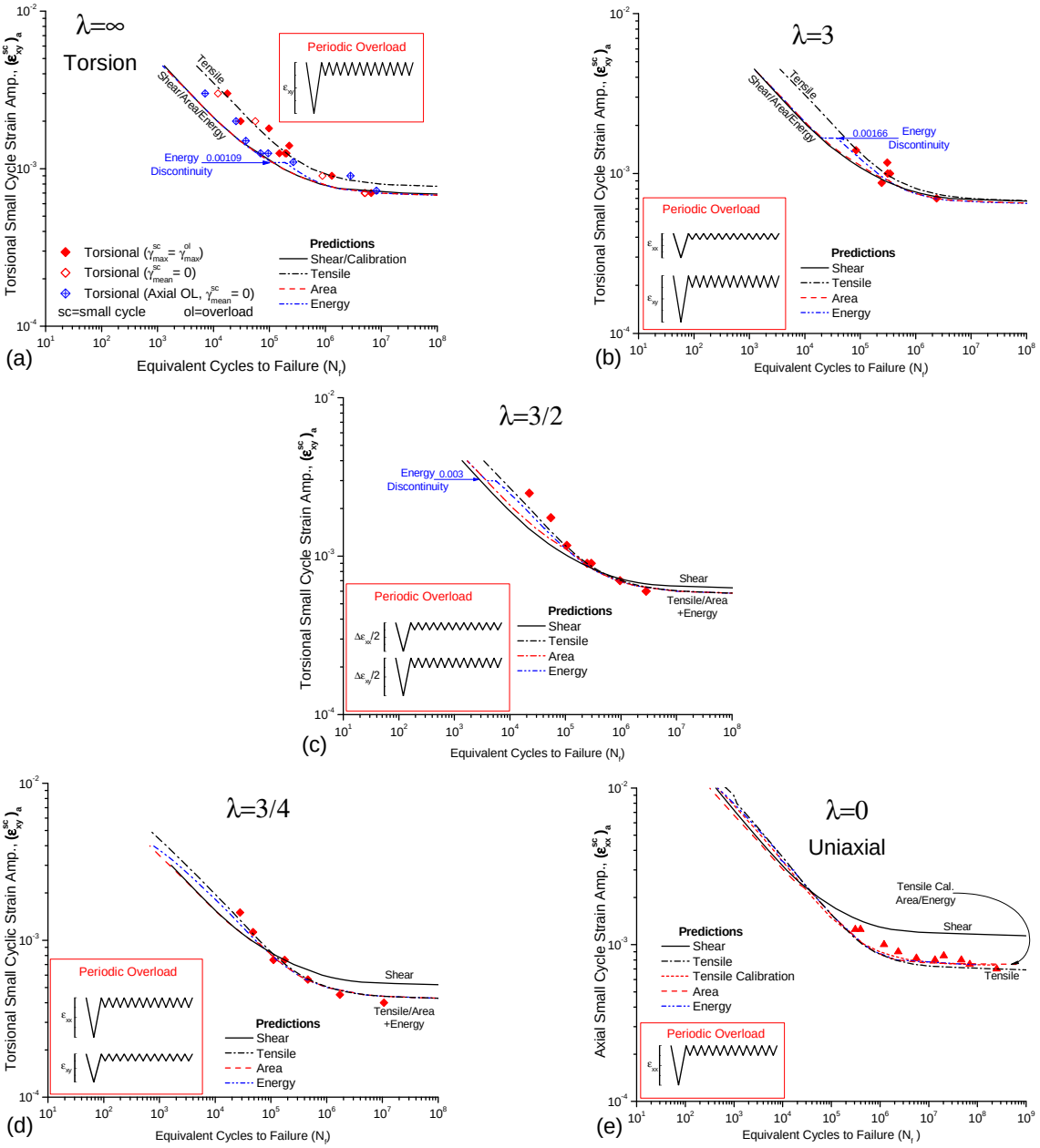

Figure 5. Life predictions made with the Area, Energy, Shear and Tensile models.

rates [12]. Because the mode I and II crack growth rates are almost equal, the differences in fatigue lives predicted by the models using the area and energy fatigue criteria is small. The experiments also support a hypothesis that the driving forces for shear and tensile crack growth are almost the same since the cracks in a few of the specimens tested at each strain ratio repeatedly alternated between growth on shear planes and growth on tensile planes.

Both the area and energy life gave predictions close to the observed fatigue lives. However, the fatigue life predictions become more conservative at short lives (higher

strain amplitudes) and higher biaxial strain ratios. During the course of generating the mode II crack growth rate data the growing shear crack occasionally bifurcated (this became more frequent as the stress intensity range increased) and decreased the crack growth rate significantly. Crack growth rate data obtained during the period following crack bifurcation was eliminated from the dataset, so that the crack growth rates used to construct the crack growth rate curves were higher than the average crack growth rates. The consequence of using a higher crack growth rate curve is an overestimate of crack growth rates and a correspondingly shortened fatigue life prediction.

CONCLUSIONS

Two crack growth models predicted both the crack-face interference-free fatigue life and the maximum length of shear cracks observed in smooth tubes tested under in-phase biaxial loading – these models followed the growth of a crack from a shallow but long crack of persistent slip-band depth to the failure length. The two models changed the crack growth plane based on the strain energy release rate (energy) and the maximum crack growth rate (area) criteria. It was determined that:

1. Both models satisfactorily predicted the fatigue life of the smooth tubes for the biaxial strain ratios examined in this study ($\lambda = \varepsilon_{xy}/\varepsilon_{xx} = \infty$, 3, 3/2, 3/4, and 0): neither predicted the life data substantially better than the other, and they both provided better predictions across the range of strain ratios than models in which all the crack growth was assumed to be confined to either the planes of maximum shear or planes of maximum tension.
2. Both models qualitatively predicted the maximum shear crack length trends: increased strain ratio and/or increased small cycle strain amplitudes led to longer maximum shear crack lengths.
3. The energy (strain energy release rate) model and the area (crack growth rate) model provided reasonable estimates of the upper and lower bounds, respectively, of the intermediate shear crack length region ($50\mu m$ to $15mm$).
4. The difference in the maximum shear crack length predictions at the time of mode change between the two models and the close proximity of their respective fatigue life predictions to each other are assumed to be the result of almost equal tensile and shear mode crack growth rates.

REFERENCES

1. Elber, W. (1970). *Engineering Fracture Mechanics* **2**(1), 37–45.
2. Elber, W. (1971). In: *Dam. Tol. in Aircraft Struct.*, ASTM STP 486, pp. 230–242, Amer. Soc. Test. Mat., Phil.
3. DuQuesnay, D. L., Topper, T. H., Yu, M. T. and Pompetzki, M. A. (1992). *Int. J. Fat.* **14**(1), 45–50.

4. Hopper, C. and Miller, K. (1977). *Journal of Strain Analysis* **12**(1), 23–28.
5. Bonnen, J. J. F. and Topper, T. H. (1999). *Int. J. Fat.* **21**(1), 23–33.
6. Kaufman, R. P. and Topper, T. H. (2003). In: *Biax./Multiax. Fat. and Fract.*, ESIS STP 31, pp. 123–146. Elsevier Int. Ser. on Struct. Integ., 31, ISBN: 0-08-044129-7.
7. Jurcevic, R., DuQuesnay, D. L., Topper, T. H. and Pompetzki, M. A. (1990). *Int. J. Fat.* **12**(4), 259–266.
8. Bonnen, J. J. F. and Topper, T. H. (1999). In: *Multiax. Fat. & Deform.: Test. & Pred.*, Kalluri, S. and Bonacuse, P. J., eds., ASTM STP 1387, pp. 213–231, Amer. Soc. Test. Mat., Phil.
9. Varvani-Farahani, A. and Topper, T. H. (1999). *Fat. Frac. Eng. Mat. Struct.* **22**(8), 697–710.
10. Socie, D. and Leese, G. (Eds.) (1989). *Multiaxial Fatigue: Analysis and Experiment*, AE-14, Soc. of Automotive Engineers.
11. Cordes, T. and Lease, K. (Eds.) (1999). *Multiaxial Fatigue of an Induction Hardened Shaft*, AE-28, Soc. of Automotive Engineers, Warrendale, PA.
12. Bonnen, J. J. and Topper, T. H. (2006). In: *Proc. Int. Conf. on Crack Paths, 2006*, CP 2006, European Struct. Integ. Soc., Parma, Italy. In this conference proceeding.
13. Bonnen, J. J. F., Topper, T. H. and Conle, F. A. (2001). *Int. J. Fat.* **23**(S1), 385–394.
14. Socie, D., Hua, C. and Worthem, D. (1987). *Fat. Frac. Eng. Mat. Struct.* **10**(1), 1–16.
15. McEvily, A. (1970). In: *Air Force Conference on Fatigue and Fracture of Aircraft Structures and Materials*, AFFDL-TR 70-144, pp. 451–456.
16. Abdel-Raouf, H., Topper, T. and Plumtree, A. (1991). *Scripta Metallurgica et. Materialia* **25**, 587–602.
17. Abdel-Raouf, H., Topper, T. and Plumtree, A. (1992). *Fat. Frac. Eng. Mat. Struct.* **15**(9), 895–909.
18. Raju, I. and Newman, J. (1986). In: *Fracture Mechanics: Seventeenth Volume*, ASTM STP 905, pp. 789–805, Amer. Soc. Test. Mat.
19. Irwin, G. (1962). *Journal of Applied Mechanics, ASME* **29**, 651–654.
20. Green, A. and Sneddon, I. (1950). *Proceedings of the Cambridge Philosophical Society* **46**, 159–164.
21. Kassir, M. and Sih, G. (1966). *Journal of Applied Mechanics, ASME* **33**, 601–611.
22. Lakshminarayana, H. and Murthy, M. (1976). *Int. J. Fract.* **12**, 547–566.
23. Palaniswamy, K. (1972). Ph.D. thesis, California Institute of Technology, Pasadena, California.
24. Nuismer, R. (1975). *Int. J. Fract.* **11**, 245–250.
25. Griffith, A. (1920). *Phil. Trans. Royal Soc. London* **A221**, 163–198.
26. Hourlier, F. and Pineau, A. (1982). In: *Advances in Fracture Research Fracture 81*, volume 4, Francois, D., ed., pp. 1833–1840, Pergamon Press, Oxford. Held in Cannes, March 29 – April 3, 1981.